Radial distribution of the end-to-end distance of linear stiff chains

Jangnyeol Moon
Department of Physics, Third Military Academy, Yungchun, Kyungbook 771-849, Korea

Sang Bub Lee
Department of Physics, Kyungpook National University, Taegu 702-701, Korea

(Received 30 October 1995)

The radial distribution of the end-to-end displacement of linear stiff chains embedded on a discrete lattice shows a peculiar character that some peaks appear at different places in a certain limit. This limit imposes both the stiffness and length of the chain to be infinite while their product, as duely defined, is being constant. We model the chain as the persistent random walk (PRW) and obtain the distribution functions by Monte Carlo simulations on square, cubic, and diamond lattices. Explanations on why the peaks occur at particular places depending on the type of lattice are given with detailed calculations for the height of peaks in the case of the square and simple cubic lattices. For the completeness we present the results for two types of the randomly broken chain models (RBC-I and -II), i.e., off-lattice versions for the stiff chain, obtained from much more extensive simulations than those previously reported. [S1063-651X(96)01408-0]

PACS number(s): 05.40.+j, 05.50.+q, 64.60.Fr

I. INTRODUCTION

The stiffness of a linear polymer in equilibrium is usually determined by the competing effect of the energetics between isomeric states and the thermal energy [1–3]. If an isomeric state is such that the chemical bond of an added monomer favors a particular local orientation more than others, the chain tends to grow ''straight.'' [For real polymers like polyethylene having a zigzag structure of spinal carbon atoms or like polyisocyanates [4,5] and DNA's having the helicity, the straightness should be viewed in a scale larger than individual monomers.] The straight part of the chain is termed a segment and the mean length of the segment the *persistence length*. Hence the stiffer the chain, the longer its persistence length and it becomes rodlike if the degree of polymerization is low enough. For theoretical treatment and computer simulation of stiff linear chains embedded on discrete lattices, one can adopt the persistent random walk (PRW) model [6,7]: the first step starting at the origin is made to any of the nearest neighbor sites with an equal probability but all the subsequent steps are made either in the same direction as the preceding one with probability $1-p$ (*trans* steps) or in one of the other directions with probability p divided by the number of such directions (*gauche* steps), with the backtracking being always precluded. [The step size, i.e., the lattice constant is set to be 1.]

Thus, in the framework of the PRW model, the gauche probability p is the only parameter that controls the stiffness represented by, e.g., the persistence length $l_p=p^{-1}$ or the mean number of segments $Np+1$ in N-step walks. An analytic expression of the mean squared end-to-end distance of the PRW is known, which reduces to $\langle R^2\rangle=2(e^{-Np}+Np-1)/p^2$ in the so-called stiff limit [7–9]

$$p\to 0, \quad N\to\infty, \quad Np=\text{ const.} \tag{1}$$

Two kinds of limiting behaviors can easily be picked up, that is, the rodlike regime corresponding to $Np\ll 1$ where the radial distribution approaches to a δ function peaked at $R=N$, and the Gaussian regime corresponding to $Np\gg 1$ with a Gaussian radial distribution. These behaviors are qualitatively unchanged in three or higher dimensions even in the presence of the excluded-volume effect [7,9–11].

It has been found that, in the crossover regime where Np is of the order of unity, the distribution function has peculiar jumps and peaks [12,13,11]. We note that such jumps and peaks appear on different places depending on the types of lattices on which the model is embedded. Unfortunately, the full knowledge of the cause of such jumps and peaks has not been revealed up to date, as far as we know.

In this paper, we present the full explanations of why such peaks occur at particular places. We present the detailed calculations for the height of peaks in the case of square (sq) and simple cubic (sc) lattices and for the exact positions of such peaks for body-centered cubic (bcc), face-centered cubic (fcc), and diamond lattices. We also present the results for two types of off-lattice versions of stiff chain, termed the randomly broken chain model (RBC-I and II), obtained from extensive Monte Carlo calculations. It should, however, be noticed that although we limit our work only on the positions and the heights of the peaks, a qualitative investigation of the widths of such peaks and heights is also a necessary part of the work for the full knowledge of the peaks.

The probability density distribution of end-to-end displacement of the N-step PRW can be expressed as

$$W_N(\mathbf{r})=\frac{1}{z}\sum_{t=0}^{N-1} g_N(t,\mathbf{r})\left(\frac{p}{z-2}\right)^t(1-p)^{N-1-t}, \tag{2}$$

where z is the coordination number of the lattice and $g_N(t,\mathbf{r})$ is the number of N-step walks with t gauche steps whose end-to-end displacement is $\mathbf{r}$. We define the radial distribution or the probability density function as a continuous histogram of width $\Delta R\equiv N/A$, A being an integer, centered at $r=R=n\Delta R$ $(n=0,1,2,\ldots,A)$

$$P_N(R)=\frac{1}{\Delta R}\sum_{R-\frac{\Delta R}{2}\le r<R+\frac{\Delta R}{2}} W_N(\mathbf{r}). \tag{3}$$

We choose $p=0.01$ and $N=A=500$ ($\Delta R=1$) in the following discussions since these parameters well meet both conditions for the crossover regime and the stiff limit (1) on the computational efficiency.

In Sec. II, the structures of $P_N(R)$ for sc and sq lattices are analyzed, focusing on the positions of the peaks and jumps, and a detailed calculation is performed for the height of the peaks. In Sec. III, we present the results for the bcc, fcc, and diamond lattices in a similar vein. Section IV contains the results for two off-lattice versions of stiff chains obtained from much more extensive simulations than those previously reported. Section V is devoted to the summary and concluding remarks.

II. RESULTS FOR SIMPLE CUBIC AND SQUARE LATTICES

In Fig. 1(a), we present the radial distributions of the PRW's on sc (solid line) and sq lattices (dotted line) obtained from 10×10^6 walks generated for each lattice by Monte Carlo simulations. The ordinate R is scaled by N, i.e., by the fully stretched length, to indicate that the shape of the curve is identical for the same Np in the stiff limit (1). We note that there are two peaks at $R=N$ and $N/\sqrt{2}$ for both lattices and a jump at $R=N/\sqrt{3}$ for the sc lattice only. This feature remains unchanged if the value of Np varies within the same order of magnitude, i.e., in the crossover regime.

The peak at $R=N$ can easily be understood [12,13,11] considering that the probability for the walks of all trans steps is finite by Eq. (2) in limit (1), which is $e^{-Np}\approx0.0067$ for $p=0.01$ and $N=500$.

The peak at $R=R_0=N/\sqrt{2}$, on the other hand, turns out to be due to a group of walks whose steps are made in either of two mutually perpendicular directions [e.g., $+x$ and $+y$ directions in Fig. 1(b)]. These *planar* walks end up at a boundary edge of the set of lattice points that an N-step PRW can reach with a nonzero probability and R_0 is the shortest distance from the origin to the edge [see Fig. 1(b)]. Figure 2(a) shows the edge and some walks whose steps are made either in $+x$ or $+y$ direction. As the radius increases passing R_0, these walks start to contribute to the distribution function: the first contribution comes from the walks that end at the points in ''shell 1,'' second from those in ''shell 2,'' and so on. Although the number of points to be reached with a nonzero probability in ''shell 1'' is smaller than those in ''shell 0'' (the inner shell of shell 1), the new contribution of these edge points is large enough to result in a sudden increase in the distribution function thereat because the edge points are reached with smaller number of turns, hence, with higher probabilities.

The main reason why the peak is so sharp is that the length of the edge that subsequent shells contain rapidly decreases as their radius increases. For example, one can check that the portion of the edge in ''shell 2'' ($\overline{P_1P_2}$) is only about 40% of that in ''shell 1'' ($\overline{P_0P_1}$) for large A. Moreover the number of ways to reach an edge point decreases as its distance increases, which must cooperate for the sharpness of the peak.

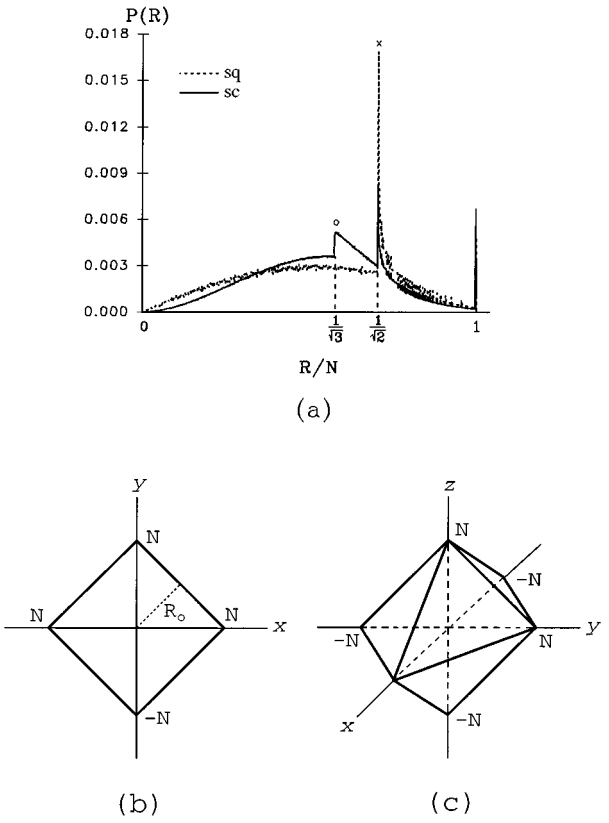

FIG. 1. (a) Radial distributions of the N-step persistent random walks (PRW's) on square (dotted line) and simple cubic (solid line) lattices. 10×10^6 samples were generated by Monte Carlo simulation for each lattice and the histograms of interval $\Delta R=1$ were obtained with statistical fluctuations less than or comparable to the local jagged structure of each curve. The cross ($\times$) indicates the boundary edge contribution and the circle ($\bigcirc$) the boundary plane contribution. (b) The boundary square on a square lattice beyond which an N-step walk cannot reach. R_0 is the (shortest) distance from the origin to a side. (c) The octahedron on a simple cubic lattice beyond which an N-step walk cannot reach. R_1 (not shown) is the distance from the origin to a face. Note that $R_0=N/\sqrt{2}$ and $R_1=N/\sqrt{3}$.

One can estimate the height of the peak assuming that it is determined by the contribution of edge points in ''shell 1.'' The height of the peak H_P can be formally written as

$$H_P=\frac{z(z-2)}{2}\sum_{\mathbf{r}\in\overline{P_1P_1'}}\sum_{t=1}^{N-1}\mathcal{P}_t(\mathbf{r}), \tag{4}$$

where $\mathcal{P}_t(\mathbf{r})$ is the probability for an N-step PRW to reach $\mathbf{r}$ by making t turns (gauche steps), and the first summation is over all edge points in ''shell 1.'' The factor $z(z-2)/2$ comes from that there are that number of equivalent boundary edges (''equivalent'' in the sense of symmetry). If we approximate $\mathcal{P}_t(\mathbf{r})$ by $\mathcal{P}_t(P_0)$ substituting $\mathbf{r}$ with a representative point P_0, then the first summation in Eq. (4) reduces to mn_tW_t, where $m=(2\sqrt{2}/A)^{1/2}N$ is the number of points in the edge $\overline{P_1P_1'}$, n_t the number of ways to reach the point

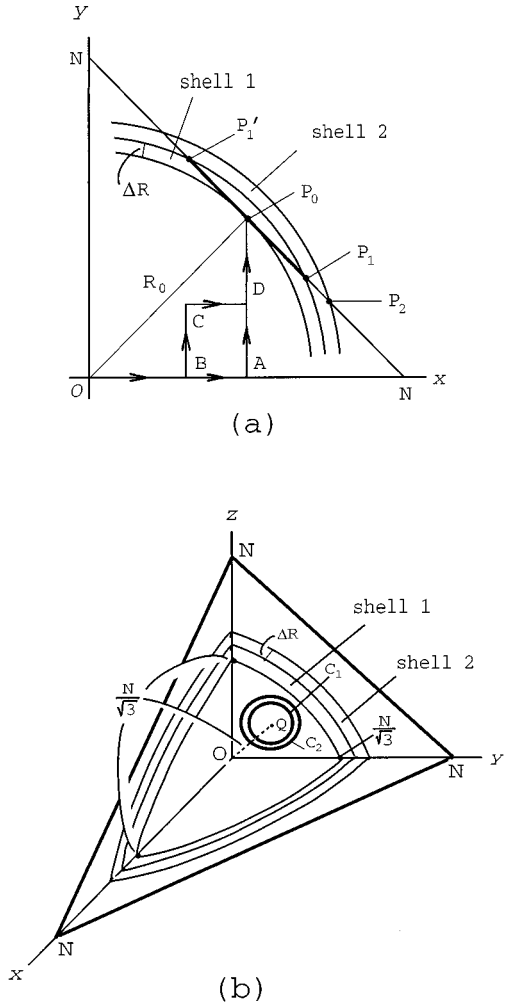

FIG. 2. (a) A diagram for explaining the boundary edge contribution. The probability for an N-step PRW to reach lattice points on $\overline{P_1P_1'}$ falling in ''shell 1'' is responsible for the peak ($\times$) in Fig. 1(a). Path $OBCDP_0$ is an example of a three-turn PRW to reach the representative point P_0. (b) A diagram for explaining the boundary plane contribution. The probability for an N-step PRW ending on each lattice point inside the ''shell 1'' is responsible for the jump ($\bigcirc$) in Fig. 1(a). The representative point Q is the contact point between the inner surface of shell 1 and the octahedral face.

P_0, and $W_t=z^{-1}[p/(z-2)]^t(1-p)^{N-1-t}$ the weighting for any path to P_0 with t gauche steps. Moreover because of the symmetry n_t can be written as $2n_t'$, n_t' being such that the first step is predetermined along, e.g., $+x$ direction as in Fig. 2(a). Thus Eq. (4) can be recast as

$$H_P\approx\left(\frac{2\sqrt{2}}{A}\right)^{1/2}Np\sum_{t=1}^{N-1}n_t'\left(\frac{p}{z-2}\right)^{t-1}(1-p)^{N-1-t}. \quad (5)$$

Here n_t' is equal to the number of ways to choose $t-1$ turning points, e.g., the points B and C in Fig. 2(a) for the path $OBCDP_0$ for $t=3$ (note that the last point D is uniquely determined by the preceding two points). We obtain up to $t=5$

$$n_1'=1,$$

$$n_2'=\frac{N}{2}-1\approx\frac{N}{2},$$

$$n_3'=\left(\frac{N}{2}-1\right)^2\approx\frac{N^2}{4},$$

$$n_4'=\sum_{x=1}^{\frac{N}{2}-2}\left(\frac{N}{2}-1-x\right)\left(\frac{N}{2}-1\right)\approx\frac{N^3}{16},$$

$$n_5'=\left[\sum_{x=1}^{\frac{N}{2}-2}\left(\frac{N}{2}-1-x\right)\right]^2\approx\frac{N^4}{64},$$

which, when substituted in Eq. (5), give in limit (1)

$$H_P\approx\left(\frac{2\sqrt{2}}{A}\right)^{1/2}Npe^{-Np}\left[1+\frac{Np}{2(z-2)}+\frac{(Np)^2}{4(z-2)^2}+\frac{(Np)^3}{16(z-2)^3}+\frac{(Np)^4}{64(z-2)^4}\right]. \quad (6)$$

Having higher order terms, one may find that H_P is written as a power series of $x\equiv Np/(z-2)$ and $x>1$ from our choice of $Np=5$ which makes the power series appear ill defined. However, we believe that the series does converge due to the numerical factor in the denominator in each term. Estimated from Eq. (6) are 0.55×10^{-2} for the sc lattice and 1.37×10^{-2} for the sq lattice and we see that these values agree reasonably well with the Monte Carlo data in Fig. 1(a).

We note another interesting feature of the radial distribution, a jump occurring at $R_1=N/\sqrt{3}$ for the sc lattice which is absent for the sq lattice. We identify R_1 as the distance from the origin to the octahedral planes forming the boundary beyond which the N-step PRW cannot reach [see Fig. 1(c)]. If a walk consists of steps made in either of the three mutually perpendicular directions, it will end up at a point on a boundary octahedral plane. Figure 2(b) shows the plane cutting through $+x$, $+y$, and $+z$ axes each at N, two consecutive shells of thickness ΔR, and the intersections between the plane and shells, i.e., the contact point Q between the plane and the inner surface of shell 1, and the intersection circles C_1 and C_2 between the plane and the outer surfaces of shells 1 and 2, respectively. Thus, as the end-to-end distance increases passing $R=R_1$, walks terminating at the boundary planes start to contribute to the distribution function, producing a sudden jump thereat.

For the same reason as discussed for the peak at $R=R_0$, the height of the jump can be considered coming dominantly from the probability of the walk to reach the points inside the circle C_1. We note that the peak introduced by this jump is not so sharp as the one at $R=R_0$. This is because the number of points of boundary plane contained in the subsequent shells varies little (in fact, it increases very slowly) as the radius of the shell increases and distant points are only entropically less favorable. In a manner similar to Eq. (4), we write the height of the jump H_J as

$$H_J=\frac{z(z-2)(z-4)}{3!}\sum_{\mathbf{r}\ \text{in}\ C_1}\sum_{t=1}^{N-1}\mathcal{P}_t(\mathbf{r}), \quad (7)$$

where the factor before the summations is the number of equivalent polyhedral planes for general hypercubic lattices and the first sum runs over all end points inside the circle C_1. We approximate this equation by replacing $\mathbf{r}$ by a representative point Q, reducing the first summation to mn_tW_t as for the peak at R_0, where in this case $m=2\pi N^2/3A$. Again by symmetry, n_t can be written as $6n_t'$, n_t' being the number of ways to reach the point Q by making t turns with directions of the first step and first turn predetermined along $+x$ and $+y$, respectively. Thus Eq. (7) can be recast as

$$H_J \approx \left(\frac{z-4}{z-2}\right)\frac{2\pi}{3A}(Np)^2\sum_{t=2}^{N-1} n_t'\left(\frac{p}{z-2}\right)^{t-2}(1-p)^{N-1-t}. \tag{8}$$

We obtain, up to $t=5$,

$$n_2'=1,$$

$$n_3'=\left(\frac{N}{3}-1\right)\times 2\approx\frac{2N}{3},$$

$$n_4'=\left(\frac{N}{3}-1\right)^2\times 4\approx\frac{4N^2}{9},$$

$$n_5'=5\left(\frac{N}{3}-1\right)^3+3\sum_{x=1}^{N/3-2}\left(\frac{N}{3}-1-x\right)\left(\frac{N}{3}-1\right)\approx\frac{13N^3}{54},$$

which, when substituted in Eq. (8), give in the stiff limit (1)

$$H_J\approx\left(\frac{z-4}{z-2}\right)\frac{2\pi}{3A}(Np)^2e^{-Np}\times\left[1+\frac{2Np}{3(z-2)}+\frac{4(Np)^2}{9(z-2)^2}+\frac{13(Np)^3}{54(z-2)^3}\right]. \tag{9}$$

We found that the estimate for the sc lattice 1.06×10^{-3} amounts to about 70% of the Monte Carlo result in Fig. 1(a) but approaches more than 90% for the four-dimensional hypercubic lattice (not shown).

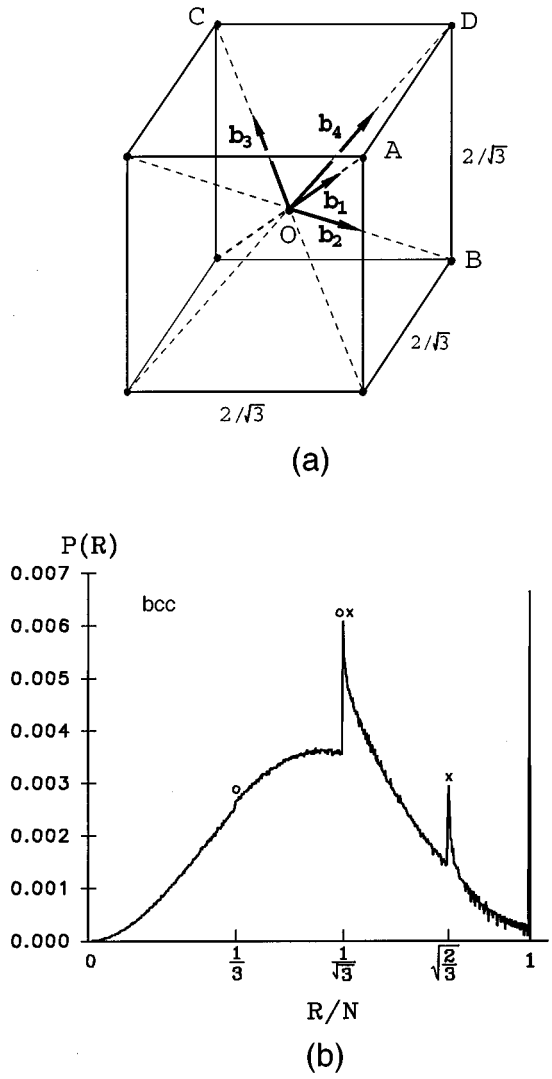

FIG. 3. (a) A unit cube of the bcc lattice centered at the origin with coordination vectors $\mathbf{b}_i$. The end points of N-step PRW's on the bcc lattice constitutes a cube of side $(2/\sqrt{3})N$. (b) As Fig. 1(a) for the PRW on the bcc lattice.

III. RESULTS FOR BCC, FCC, AND DIAMOND LATTICES

In this section we determine only the exact positions of peaks and jumps appearing on the bcc, fcc, and diamond lattices, employing essentially the same arguments as given in the preceding section. We can, in principle, perform similar calculations to estimate the heights of those features if necessary.

Figures 3, 4, and 5 show the Monte Carlo data of the radial distributions for the bcc, fcc, and diamond lattices, respectively, obtained from 10×10^6 PRW's for each case. The peak at $R=N$ is again due to the finite probability for the walks of no gauche step, regardless of the lattice type. By now, we know that the peaks and jumps at different positions are due to contributions of the boundary edge and plane on which N-step walks end and that those edges and planes cut at distance N through a set of ''coordinate axes,'' chosen in directions of corresponding coordination vectors. We will identify such a set of ''coordinate axes'' for *all* peaks and jumps and find distances from the origin to the corresponding edges and planes.

In Fig. 3(a), a unit cube of the bcc lattice is shown with four coordination vectors, out of a total of eight, indicated by $\mathbf{b}_i$. Since the lattice constant is chosen to be unity the length of each edge is $2/\sqrt{3}$. Each boundary *edge* is determined by a pair of ''coordinate axes'' in directions of any two noncolinear coordination vectors, i.e., there are $z(z-2)/2=24$ such pairs. If we take this cube for geometry of the scaled (N-step) PRW by the stretched length N, these edges can be identified as domain boundaries of walks and can be obtained by connecting the pairs of vertex points of the cube. For example, the edge $\overline{AB}$ is determined by axes in directions of $\mathbf{b}_1$ and $\mathbf{b}_2$ and $\overline{BD}$ by $\mathbf{b}_2$ and $\mathbf{b}_4$, and so on. These edges are classified as the two distinct ones, each having 11 more equivalents, the distances of which are $1/\sqrt{3}$ and $\sqrt{2/3}$, respectively. Thus these contributions of two types of boundary edges give rise to the peaks at $R=N/\sqrt{3}$ and $\sqrt{2/3}N$ in the original scale, as shown in Fig. 3(b).

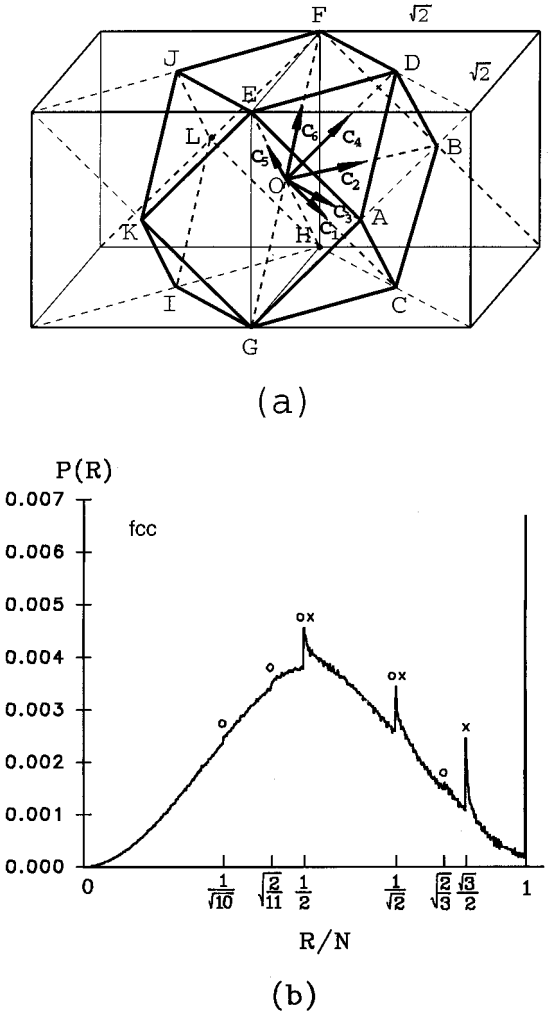

FIG. 4. (a) A pair of unit cubes of the fcc lattice centered at the origin with coordination vectors $\mathbf{c}_i$. The 14-faced polyhedron indicated by thick lines connecting the twelve sites nearest to the origin forms the domain of N-step PRW scaled by N. (b) As Fig. 1(a) for the PRW on the fcc lattice.

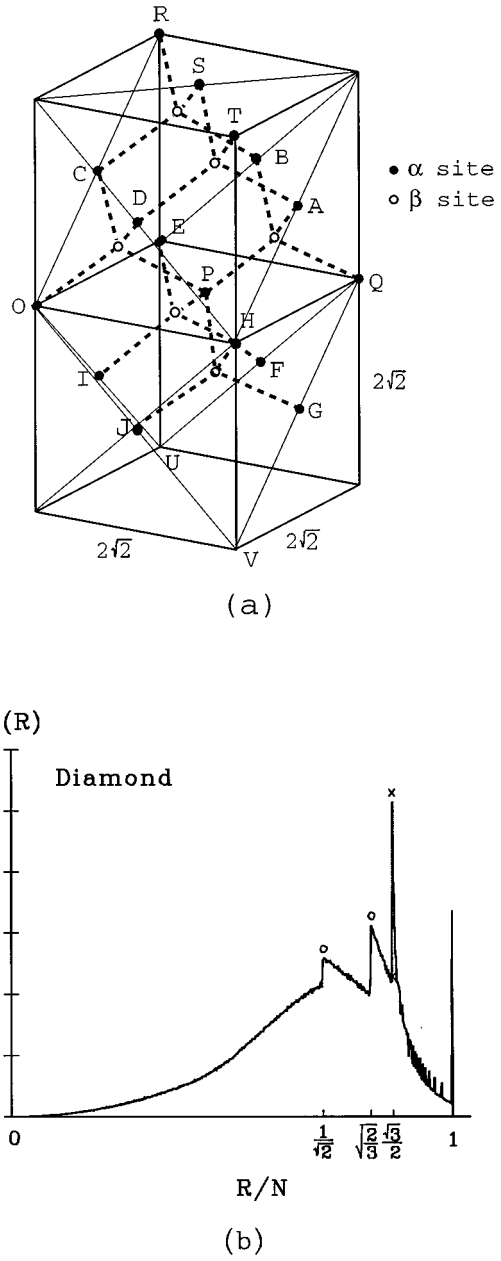

FIG. 5. (a) A pair of unit cubes of diamond lattice. The two (fcc) sublattice nature is indicated by α (filled circle) and β (open circle) sites. A *trans* step is defined as such that it forms a plane with its two immediately preceding steps. (b) As Fig. 1(a) for the PRW on the diamond lattice.

Similarly, the rescaled boundary *planes* can be obtained by connecting triplets of vertices of the cube, e.g., $\triangle ABC$ determined by axes in directions of $\mathbf{b}_1$, $\mathbf{b}_2$, and $\mathbf{b}_3$ and $\triangle ABD$ by $\mathbf{b}_1$, $\mathbf{b}_2$, and $\mathbf{b}_4$. There are two distinct planes out of $z(z-2)(z-4)/6=32$, 8 of which are equivalent to $\triangle ABC$ and 24 to $\triangle ABD$ whose distances are, respectively, $\frac{1}{3}$ and $1/\sqrt{3}$. Thus these two kinds of boundary plane contributions produce jumps at $R=N/3$ and $N/\sqrt{3}$, as shown in Fig. 3(b).

We note that the *true* boundary for the N-step PRW on the bcc lattice is the surface of a cube of side $(2/\sqrt{3})N$ in the sense that the walk cannot reach beyond the boundary. But we still called the internal plane $\triangle ABC$ ''boundary'' not just for convenience but it *is* for a set of walks grown in particularly chosen directions. The features for the bcc lattice are less prominent compared to those of the sq and sc lattices. This is mainly because the coordination number of the bcc lattice is larger [see Eqs. (5) and (8)]. We also note that the two kinds of contributions appear coincidentally at $R=N/\sqrt{3}$ and that the jump at $R=N/3$ is so small as to be barely noticeable. The reason for the latter is that the density of the lattice point on that plane is small and, in addition, the distance of the plane is too short to yield a large ''circle C_1'' [as in Fig. 2(b)], let alone a larger z.

Figure 4(a) shows a pair of unit cubes of the fcc lattice, with the coordination vectors indicated by $\mathbf{c}_i$'s. The length of the edge of the cube is $\sqrt{2}$ and the 12 nearest-neighbor sites of site O are labeled by letters ''A'' through ''K'' which constitute the 14-faced polyhedron indicated by thick lines. The sides and faces of this polyhedron, when blown up by a factor of N for N-step PRW, form the true boundaries containing some ''internal'' ones as in the case of the bcc lattice.

Even though there are 60 pairs of coordinate axes gener-

ating a boundary edge, only three are distinct: when rescaled to the unit cube with the origin positioned at O, axes $\overline{OG}$ and $\overline{OA}$ form an edge $\overline{GA}$, axes $\overline{OG}$ and $\overline{OB}$ an edge $\overline{GB}$, and axes $\overline{OG}$ and $\overline{OH}$ an edge $\overline{GH}$, the distance of which are, respectively, $\sqrt{3}/2$, 1/2, and $1/\sqrt{2}$. Twenty-four out of sixty boundary edges are equivalent to each of the first two edges and the rest to the third one. The peaks due to these contributions are shown in Fig. 4(b) at $R=N/2$, $N/\sqrt{2}$, $(\sqrt{3}/2)N$. The reason why the height of the peak at $R=(\sqrt{3}/2)N$ is greatest is that, in addition to a relatively large number of equivalent edges, the density of points on the edge is largest and the part of the edge in ''shell 1'' [as $\overline{P_1P_1'}$ in Fig. 2(a)] is larger as R gets larger.

The boundary planes for the fcc lattice are generated by 160 triplets of noncolinear coordination vectors, 16 out of which are coplanar, e.g., $(\mathbf{c}_1,\mathbf{c}_3,\mathbf{c}_5)$ or $(\mathbf{c}_1,\mathbf{c}_4,\mathbf{c}_6)$, whose contributions to producing jumps in the distribution function are negligible (with the weight proportional to p). As far as the distance of the boundary planes from the origin is concerned, we find that there are only five distinct planes. These can be identified in Fig. 4(a) as follows: $\triangle GHC$ at a distance $1/\sqrt{2}$, $\triangle GHA$ at 1/2, $\triangle GHD$ at $1/\sqrt{10}$, $\triangle GCA$ at $\sqrt{2/3}$, and $\triangle GBD$ at $\sqrt{2/11}$. These contributions are indicated in Fig. 4(b) but they are again so small as to be barely noticeable, as for the bcc lattice for similar reasons.

For the diamond lattice, where the angle between adjacent bonds is $\cos^{-1}(-\frac{1}{3})\approx 109°$, the definitions of the trans and gauche steps should be slightly modified. A step is called *trans* if it is coplanar with its two adjacent preceding steps and *gauche*, otherwise. Because of the two (fcc) sublattice nature of the diamond lattice, all the odd-numbered steps occupy a site of one sublattice and all the even-numbered steps a site of another sublattice. We call these two sublattice sites α and β, denoted by filled and open circles, respectively. For the sake of convenience we take N to be even and the lattice constant to be $\sqrt{3/2}$, so that the ''sublattice constant'' corresponding to two steps is 2, the side of the cubes shown in Fig. 5(a) is $2\sqrt{2}$, and the end-to-end distance of the walks of all trans steps is just N.

It is somewhat tricky to find the relevant boundary edges and planes for the N-step walks on a diamond lattice. Since N is taken even, the end points must be in the same sublattice as the starting point, forming the same solid figure as in the case of the fcc lattice in Fig. 4(a). However, not all the boundary edges and planes thereof give rise to peaks or jumps on the distribution function because, to do that, such ''edges'' must be able to be reached by walks of only one gauche step and such ''planes'' by walks of only two gauche steps. We find that the edges satisfying this condition are the sides of the polyhedron in Fig. 4(a), all of which are equidistant from the origin. As for the directions of individual steps, reaching those boundary edges requires two things: first, all steps on one sublattice must be trans and second, the directions of steps on another sublattice must be either of two predetermined ones with at least one gauche step. Figure 5(a) illustrates some walks of $N=4$ with one gauche step to identify the boundary edges and their distances. Only α sites are labeled, and the β site between two adjacent α sites is unique and is not labeled. Given that the first two steps are made from O to P, there are only four possible sites that a walk can reach in the next two consecutive steps without violating the requirements stated above, i.e., sites A,B,F, and G, reaching edges $\overline{QT}$, $\overline{QR}$, $\overline{QU}$, and $\overline{QV}$, respectively. Corresponding coordinate axes can be readily identified. The distances between the origin and these edge sites are all equal to $\sqrt{12}$, and hence, for N-step walks, when multiplied by a factor of $N/4$, it becomes $(\sqrt{3}/2)N$, which is responsible for the peak at that distance in Fig. 5(b).

To identify boundary planes, we consider walks of $N=6$ with only two gauche steps which take three different coordination directions defined by a sublattice, say, α sites in Fig. 5(a). There are only two nonequivalent paths meeting this condition. Given that the first two steps are made from R to C, these two kinds of paths may be represented by $RCPH$ and $RCPF$ in directions of triplets of sublattice coordinate axes $\{\overline{RO},\overline{RQ},\overline{RT}\}$ and $\{\overline{RO},\overline{RQ},\overline{RW}\}$, respectively. [Point W, not shown, is the mirror image of point O to the plane $\triangle REQ$.] In the first kind of path, gauche steps occur only at β sites, whereas in the second, they occur at both α and β sites. Thus, the corresponding boundary planes are parallel to $\triangle OQT$ and $\triangle OQE$, whose distances from R are $\sqrt{2/3}$ and $2\sqrt{2}$, respectively. For the N-step walks, these distances become, when multiplied by a factor of $N/4$, $\sqrt{2/3}N$, and $N/\sqrt{2}$, where sudden jumps indicated by a circle ($\bigcirc$) occur in the distribution in Fig. 5(b).

It is interesting that the boundary edges and planes for the diamond lattice are the surface of the 14-faced polyhedron as shown in Fig. 4(a), namely, one type of equivalent edges and two types of triangular and square faces. Moreover the small z value makes the boundary contributions in the diamond lattice more pronounced than in other types of lattices. Schroll, Walker, and Thorpe [13] noticed the position of the peak due to the boundary edge contribution by two different approaches and, as results, they found that the distribution function of one-gauche chains is nonzero only for $R\geqslant(\sqrt{3}/2)N$ (with typographical errors therein corrected) and decreases monotonically. Their Monte Carlo result of a *freely rotating chain* with an angle of 120° between two adjacent straight segments yielded a single peak there. These results may be readily understood through the geometrical considerations taken up above.

IV. OFF-LATTICE MODELS

We have discussed so far the chains embedded on discrete lattices. In this section, we deal with two off-lattice models of stiff linear chains, termed type I and type II of the *randomly broken chain* (RBC-I and RBC-II). RBC-I was originally suggested by Molina and de la Torre [12] as a semiflexible macromolecular model: Fig. 6 shows a configuration of an RBC-I consisting of a few step vectors $\{\mathbf{b}_i\}$, whose directions are either the same as their preceding step vector with probability $1-p$ or, otherwise, completely randomly distributed over the whole solid angle. [p can still be considered as the gauche probability.] On the other hand, for the RBC-II, the polar angle, denoted by θ_i in Fig. 6, is fixed and thus the dihedral angle ϕ_i alone is random. One may view the type I and II of RBC models as the ''stiff'' versions of *freely jointed chains* and *freely rotating chains* [2], respectively.

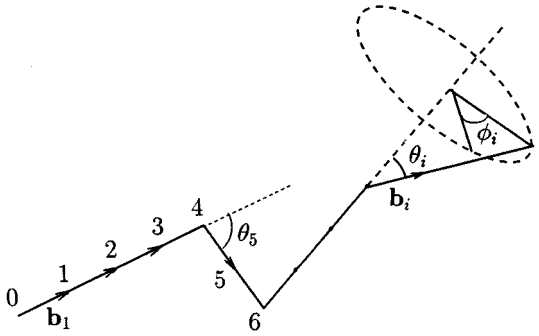

FIG. 6. A schematic configuration of the randomly broken chain (RBC) consisting of a few step vectors $\{\mathbf{b}_i\}$. The polar angle of ith step θ_i is defined as the angle between $\mathbf{b}_{i-1}$ and $\mathbf{b}_i$, while the dihedral angle ϕ_i is usually defined as the angle of rotation from a plane formed by two preceding straight segments. Trans and gauche steps defined for this case are discussed in the text.

Figure 7(a) shows the radial distributions of the end-to-end distance of the RBC-I in two and three dimensions for $p=0.01$ and $N=500$. The frequency histograms are obtained from 10×10^6 chains with an interval of $\Delta R=1$. No peak or jump appears except for $R=N$. This strongly supports that the local minima that Fig. 2 of Ref. [12] suggests are spurious except for the one near $r=L$ (in our notation, $R=N$). However, still the most important feature appears near $R=N$, as can be seen in Fig. 7(a). We note that the probability near $R=N$ is fairly large compared to the lattice results and even larger than the expected value $e^{-Np}\simeq0.0067$. The latter, as it turns out, is because of the contributions of the last interval $[N-\Delta R/2,N)$, upper bound being excluded, to the histogram. Figure 7(b), where a few chains of a single break with their first step fixed in $+x$ direction OAH, OBG, etc., are shown together with the circular loci of their end points, explains qualitatively why this contribution is large. The probability for any point on the same circle is the same in the figure. We can see that the loci are relatively concentrated near the ''surface'' of the walk domain and this might have caused the excess values on the peak at $R=N$.

For a more quantitative analysis of this feature, one may write the probability for the outermost shell, apart from the δ functionlike probability e^{-Np} at $R=N$, as

$$\mathrm{Prob}(N-\Delta L\leqslant R<N)=\sum_{t=1}^{N-1} P_{St}(\Delta L), \tag{10}$$

where $P_{St}(\Delta L)$ is the probability that an end point of an RBC-I with t breaks lies in the outermost shell of thickness ΔL, $[N-\Delta L,N)$. We then approximate the right-hand side of the above equation to a single term P_{S1} $(t=1)$, which should be reasonably good for $\Delta L\ll N$ in the limit (1). Figure 8 illustrates a chain of a single break at the end of the ith bond, whose end point hits the inner boundary of the outermost shell in which any chain of a single break with a polar angle less than θ_i falls. To the first order in ΔL,

$$\cos\theta_i=1-\frac{N}{i(N-i)}\Delta L, \tag{11}$$

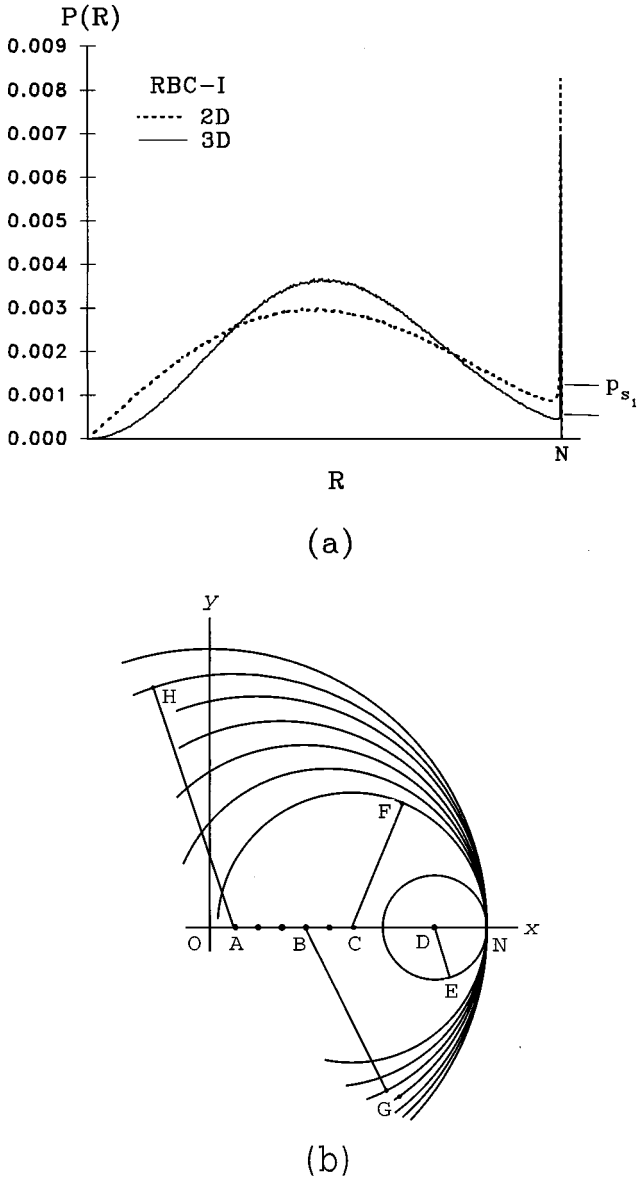

FIG. 7. (a) Monte Carlo data of the radial distribution of N-step RBC-I in two (dotted line) and three (solid line) dimensions, obtained using the parameters N, p, and ΔR the same as for Fig. 1(a). A special feature is that the probability near $R=N$ is fairly large as indicated by P_{S1}. (b) A schematic diagram for a few single-break RBC-I's with the first step $\mathbf{b}_1$ fixed in $+x$ direction, OAH,OBG, etc., and the loci of their evenly distributed end points. Each circle (or sphere in three dimensions) has the same weight $p(1-p)^{N-2}$.

which enables us to obtain expressions for $P_{S1}(\Delta L)$ in two and three dimensions

$$P_{S1}=\sum_{i=1}^{N-1}\frac{\theta_i}{\pi}p(1-p)^{N-2}$$
$$\approx\frac{pe^{-Np}}{\pi}\sum_{i=1}^{N-1}\cos^{-1}\left[1-\frac{N}{i(N-i)}\Delta L\right],\quad d=2; \tag{12}$$

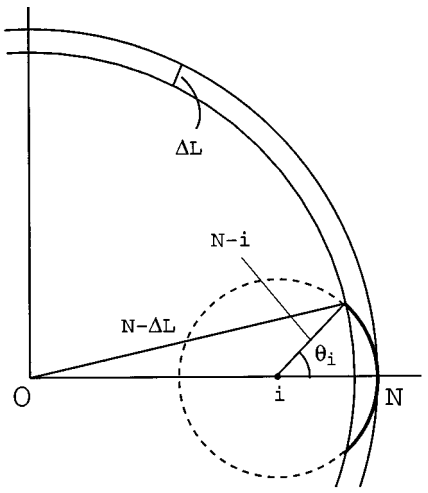

FIG. 8. An illustration of an RBC-I with a single break at $R=i$ and polar angle θ_i. End points of any chain with a polar angle less than θ_i falls in the outermost shell of thickness ΔL (indicated by a thick arc).

$$P_{S1}=\sum_{i=1}^{N-1}\frac{1-\cos\theta_i}{2}p(1-p)^{N-2}\approx pe^{-Np}(\ln N)\Delta L,\quad d=3. \tag{13}$$

It should be noted that the right-hand side of Eq. (11) may be less than -1 for some i's if ΔL is of an order of unity or larger, in which case $\cos\theta_i$ should be taken as -1 for those i's and Eqs. (12) and (13) should be changed accordingly. We found that the values obtained from Eqs. (12) and (13) are, respectively, 1.44×10^{-3} and 2.28×10^{-4} for $\Delta L=\Delta R/2=0.5$ [i.e., for the interval $[N-\Delta R/2,N)$] and that they agree with the excess values of our simulation results (at $R=N$) over the contributions of fully stretched chains, up to 90% for $d=2$ and 99% for $d=3$. [Note that simulation results are 1.61×10^{-3} and 2.31×10^{-4} for $d=2$ and $d=3$, respectively.] We performed similar comparisons for inner shells near the ''surface'' using Eqs. (12) and (13) and estimated $\mathrm{Prob}(N-1.5\Delta R\leqslant R<N-0.5\Delta R)=P_{S1}(1.5\Delta R)-P_{S1}(0.5\Delta R)\approx1.08\times10^{-3}$ for $d=2$ and 4.54×10^{-4} for $d=3$, which are about 75% and 95% of the corresponding simulation values. Therefore it seems to us that Eq. (12) is a good approximation of Eq. (10) only for $\Delta L\ll1$, while Eq. (13) is good for ΔL up to an order of unity.

We finally turn to the type II of the RBC. We note that if the gauche probability $p=1$, the RBC-II becomes a traditional *freely rotating chain* for which the second and fourth moments of the end-to-end distance are known in closed forms [2,14,15]. It can be shown that both the mean square end-to-end distance $\langle R_N^2\rangle$ and the mean square radius of gyration $\langle S_N^2\rangle$ of RBC-II have essentially the same forms as those of *freely rotating chains* and RBC-I. Since $\mathbf{R}_N\equiv\Sigma_{i=1}^N\mathbf{b}_i$, $\mathbf{b}_i$ being the ith step vector, one can write

$$\langle R_N^2\rangle=\sum_{i=1}^{N}\sum_{j=1}^{N}\langle\mathbf{b}_i\cdot\mathbf{b}_j\rangle \tag{14}$$

$$\langle S_N^2\rangle=\frac{1}{(N+1)^2}\sum_{0\leqslant i<j\leqslant N}\langle(\mathbf{R}_i-\mathbf{R}_j)^2\rangle, \tag{15}$$

where $\mathbf{R}_0=0$. Since we have for the RBC-II with polar angle θ

$$\langle\mathbf{b}_i\cdot\mathbf{b}_j\rangle=\sum_{k=0}^{|j-i|}\binom{|j-i|}{k}(\cos\theta)^k p^k(1-p)^{|j-i|-k}$$
$$=[1-p(1-\cos\theta)]^{|j-i|}, \tag{16}$$

following the well-known expressions [2] can be used to get

$$\langle R_N^2\rangle=\frac{1+\alpha}{1-\alpha}N-\frac{2\alpha(1-\alpha^N)}{(1-\alpha)^2}, \tag{17}$$

$$\langle S_N^2\rangle=\frac{N(N+2)(1+\alpha)}{6(N+1)(1-\alpha)}-\frac{N\alpha}{(N+1)(1-\alpha)^2}$$
$$+\frac{2N\alpha^2}{(N+1)^2(1-\alpha)^3}-\frac{2\alpha^3(1-\alpha^N)}{(N+1)^2(1-\alpha)^4}, \tag{18}$$

with $\alpha=1-p(1-\cos\theta)$. One can easily verify that $\alpha=\cos\theta$ (or $p=1$) for *freely rotating chains* and $\alpha=1-p$ for RBC-I and PRW on any symmetric lattices.

To investigate the radial distribution of the end-to-end displacement of the RBC-II, we generated 10×10^6 chains for each of $\theta=60°$ and $90°$, with $N=500$ and $p=0.01$ for both cases. The frequency histograms are plotted in Fig. 9. The arrows denoted are the root-mean-square of the end-to-end distance calculated from Eq. (17), and we found that they agree well with our simulation results over three or more significant digits. We also found that a peak other than the one at $R=N$ appears at $R_0=N\cos(\theta/2)$, unique for a given polar angle θ, at which chains with a single break just start to contribute to the distribution function. To elucidate this feature, we examine the geometry of single-break RBC-II's of length N shown in Fig. 10 in a similar way in some respects to Fig. 2(a). Given the first step fixed along $+x$ direction, the end points of chains lying in the first quadrant of the xy plane fall on the line $\overline{QN}$ [e.g., $O1Q$, $O(N/2)P_0$, OiP] but by the freely rotating nature of the chain they are in fact evenly distributed over separate circles on the cone as shown in the figure. A straightforward way of estimating the height of the peak is to count the number of these circles contained in the ''shell'' of thickness ΔR positioned at $R_0=\overline{OP_0}$, each contributing by the same weight. This number, say, m, is clearly the same as that of the end points on the line $\overline{P_1P_1'}$ in Fig. 10, for which we have, up to first order in ΔR, $m=\sqrt{2N\cos(\theta/2)\Delta R}/\sin(\theta/2)$. Consequently, with the single break probability $p(1-p)^{N-2}$ and $\Delta R=N/A$, the height H_P in limit (1) can be expressed as

$$H_P\approx\frac{Npe^{-Np}}{\sin(\theta/2)}\left(\frac{2\cos(\theta/2)}{A}\right)^{1/2}, \tag{19}$$

which yields an agreement with the simulation data just as well as Eq. (5) does with the simulation data for the sc lattice. To make more legitimate comparison of the estimation of Eq. (19) with a frequency histogram result, one should take into account the difference in positions of ''shells'' for

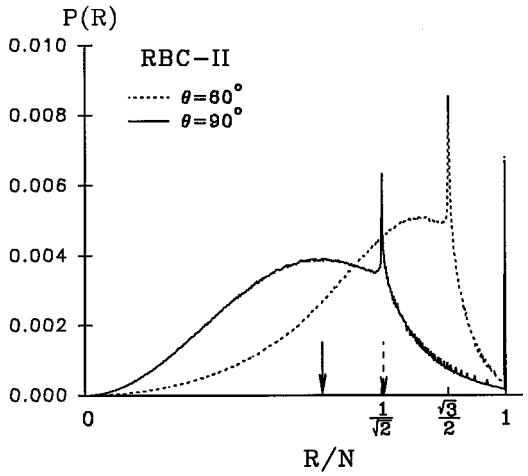

FIG. 9. The radial distributions of N-step RBC-II for polar angles $\theta=60°$ (dotted line) and $\theta=90°$ (solid line). The parameters N, p, and ΔR are the same as for Fig. 1(a). The arrows indicate the $\langle R^2\rangle$ obtained in a closed form [Eq. (17)] for each given θ.

the two cases: Eq. (19) is for $R_0 \leqslant R < R_0+\Delta R$, whereas the histogram interval in question is taken $[(n-\frac{1}{2})\Delta R,(n+\frac{1}{2})\Delta R]$ containing $R=R_0$ for some integer n. For example, for $\theta=60°$, $R_0=(\sqrt{3}/2)N\approx 433.01$ and the corresponding histogram interval is $[432.5,433.5)$, so we take $\Delta R=433.5-433.01=0.49$ for Eq. (19) and, after considering this, we found that the results agree within an error of only a few percent.

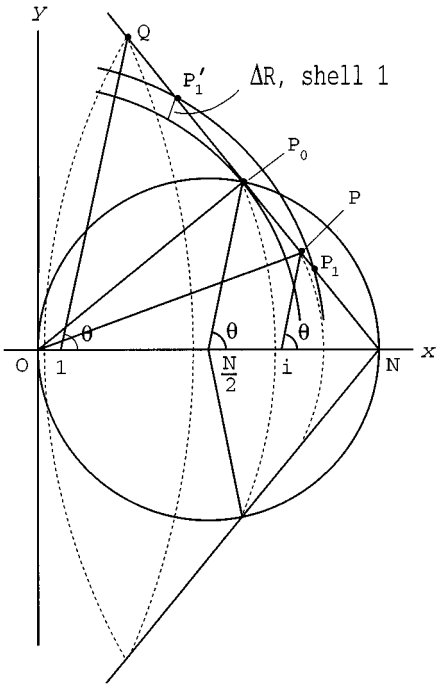

FIG. 10. A schematic diagram for three single-break RBC-II's with a polar angle θ and the first step $\mathbf{b}_1$ fixed in $+x$ direction, $O1Q$, $O(N/2)P_0$, and OiP, and corresponding circular loci of their end points on the boundary cone. A shell of thickness ΔR located at the shortest distance $R_0=\overline{OP_0}$ contains so many circles intersecting line $\overline{P_1P_1'}$ as to be responsible for the peak in Fig. 9.

An alternative way to derive Eq. (19) is to use an expression $P_1(R)$ presented in Ref. [13] for the probability density function of the single-break RBC-II, where our RBC-II is referred to as the *freely rotating chain* and our θ denoted by $180°-\theta'$. From chain OiP in Fig. 10, we have $R^2=(N-i)^2+i^2+2i(N-i)\cos\theta$ and, from $P_1(R)dR=di/N$ and taking i as a continuous variable, we get

$$P_1(R)=\begin{cases}\dfrac{1}{N\sin(\theta/2)}\dfrac{1}{\sqrt{1-(R_0/R)^2}}, & \text{if } R\geqslant R_0\equiv N\cos(\theta/2)\\ 0, & \text{otherwise.}\end{cases}$$

This $P_1(R)$ is in fact the *conditional* probability for the *single-break* chain and one needs to multiply the weight for that condition, i.e., $p(1-p)^{N-2}$ to get the right contribution to the total distribution $P(R)$. Then the height of the peak H_P due to P_1 can be estimated by an integration

$$H_P=p(1-p)^{N-2}\int_{R_0}^{R_0+\Delta R}P_1(R)dR, \tag{21}$$

which reduces to Eq. (19) in the first order of $\Delta R=N/A$.

V. SUMMARY AND CONCLUDING REMARKS

We have shown that the peaks and jumps appearing in the distribution functions of the end-to-end distance of stiff chains are due to the contributions from the boundaries beyond which the walk of a fixed number of steps cannot reach. This walk domain forms a polyhedron determined by the type of lattice in which the chain is embedded. We found out all the exact positions of the peaks and jumps for various types of lattices, which can essentially be identified as the distances from the center of the polyhedron to the boundary edges and planes. The boundary edge contribution produces a sharp peak whereas the boundary plane yields a sudden jump. In particular, for the sq and the sc lattices, we obtained approximate analytic expressions for the heights of peaks and jumps as a function of the average number of gauche steps Np in the ''stiff'' limit (1) and found that the results agree reasonably well with our Monte Carlo data.

We have also presented detailed structure of the distribution functions by Monte Carlo simulations for two off-lattice models of stiff chains, i.e., two types of the randomly broken chain (RBC-I and RBC-II), which can be viewed as the ''stiff'' versions of the randomly jointed chains and freely rotating chains, respectively. The distribution of the end-to-end distance of the RBC-I does not have any peak except at $R=N$, but the probability thereabout is considerably higher, the limiting value of which is calculated for both two and three dimensions. On the other hand, the distribution for the RBC-II shows a peak at a point other than $R=N$, which can be exactly located depending on the polar angle chosen.

We believe that our results should be directly applicable to the distribution of the mean end-to-end distances of ''real'' linear polymer chains in the stiff limit. Unfortunately up to date, however, we have not been able to find any experimental work in the literature which deals with a similar feature, except some measurements of average sizes of very

stiff polymers [5], having direct relevance to these features of the stiff chains discussed in this paper.

Besides in the experimental aspect, our results can also be considered as details of random walks with certain preferred probability distributions, i.e., the lattice random walks which tend to take a step along the same direction as that of the previous step. Since these features concern the end-to-end distance, a special type of diffusion problem or certain interaction between two functional groups attached to both end points of random walks, where the most probable, rather than the average, values of relevant variable play an important role, may find an application, a further elaboration of which is deferred to a future study.

ACKNOWLEDGMENTS

This work was supported in part by the Korea Science and Engineering Foundation under Grant No. 941-0200-035-2. The authors are grateful for this support. One of us (S.B.L.) also acknowledges the partial support from Basic Science Research Institution (BSRI 95-2405) at Kyungpook National University.

[1] P. J. Flory, *Principles of Polymer Chemistry* (Cornell University, Ithaca, 1953).
[2] P. J. Flory, *Statistical Mechanics of Chain Molecules* (Interscience, New York, 1969).
[3] P. G. de Gennes, *Scaling Concepts in Polymer Physics* (Cornell University, Ithaca, 1979).
[4] Mark M. Green, Richard A. Gross, Charles Crosby III, and Frederic C. Schelling, Macromolecules **20**, 992 (1987).
[5] H. Murakami, T. Norisuye, and H. Fujita, Macromolecules **13**, 345 (1980).
[6] J. W. Halley, H. Nakanishi, and R. Sundararajan, Phys. Rev. B **31**, 293 (1985).
[7] S. B. Lee and H. Nakanishi, Phys. Rev. B **33**, 1953 (1986).
[8] H. Nakanishi, J. Phys. (Paris) **48**, 979 (1987).
[9] J. W. Halley, D. Atkatz, and H. Nakanishi, J. Phys. A **23**, 3297 (1990).
[10] M. L. Glasser, V. Privman, and A. M. Szpilka, J. Phys. A **19**, L1185 (1986).
[11] J. Moon and H. Nakanishi, Phys. Rev. A **44**, 6427 (1991).
[12] J. J. G. Molina and J. G. de la Torre, J. Chem. Phys. **87**, 4026 (1986).
[13] W. K. Schroll, A. B. Walker, and M. F. Thorpe, J. Chem. Phys. **76**, 6384 (1982).
[14] M. F. Thorpe and W. K. Schroll, J. Chem. Phys. **75**, 5143 (1981).
[15] G. Porod, J. Polymer Sci. **10**, 157 (1953).